JACS
JOURNAL OF THE AMERICAN CHEMICAL SOCIETY

ARTICLE

pubs.acs.org/JACS

One-Electron Oxidation of Electronically Diverse Manganese(III) and Nickel(II) Salen Complexes: Transition from Localized to Delocalized Mixed-Valence Ligand Radicals

Takuya Kurahashi and Hiroshi Fujii*

Institute for Molecular Science & Okazaki Institute for Integrative Bioscience, National Institutes of Natural Sciences, Myodaiji, Okazaki, Aichi 444-8787, Japan

Supporting Information

ABSTRACT: Ligand radicals from salen complexes are unique mixed-valence compounds in which a phenoxyl radical is electronically linked to a remote phenolate via a neighboring redox-active metal ion, providing an opportunity to study electron transfer from a phenolate to a phenoxyl radical mediated by a redox-active metal ion as a bridge. We herein synthesize one-electron-oxidized products from electronically diverse manganese(III) salen complexes in which the locus of oxidation is shown to be ligand-centered, not metal-centered, affording manganese(III)−phenoxyl radical species. The key point in the present study is an unambiguous assignment of intervalence charge transfer bands by using nonsymmetrical salen complexes, which enables us to obtain otherwise inaccessible insight into the mixed-valence property. A d^4 high-spin manganese(III) ion forms a Robin−Day class II mixed-valence system, in which electron transfer is occurring between the *localized* phenoxyl radical and the phenolate. This is in clear contrast to a d^8 low-spin nickel(II) ion with the same salen ligand, which induces a *delocalized* radical (Robin−Day class III) over the two phenolate rings, as previously reported by others. The present findings point to a fascinating possibility that electron transfer could be drastically modulated by exchanging the metal ion that bridges the two redox centers.

INTRODUCTION

Mixed-valence compounds, typically bearing two bridged metal centers in different formal oxidation states, have played an important role in the study of electron transfer, which is one of the most fundamental reactions in physics, chemistry, and biology.[1] A prototypical example is the pyrazine-bridged Ru^{II}−Ru^{III} dimer, which is known as the Creutz−Taube ion.[2] A pivotal issue in mixed-valence chemistry has been the extent of the electronic interaction between two metal centers, which determines the efficiency of the intramolecular electron transfer, from Ru^{II} to Ru^{III}, for example. According to the extent of the electronic interaction, mixed-valence compounds are classified into three categories, classes I, II, and III, as proposed by Robin and Day.[3] In class I mixed-valence compounds, no electron transfer occurs when two bridged metal centers are far apart or when their interaction is symmetry or spin forbidden. In class II mixed-valence compounds, two metal centers have detectable electronic interaction and electron transfer is occurring between two metal centers. In class III mixed-valence compounds, two metal centers have such strong electronic interaction that delocalization occurs and the formal charge on each metal center is averaged, $Ru^{II.5}$−$Ru^{II.5}$, for example. Class III mixed-valence compounds are distinct from class II compounds in delocalization of the unpaired electron as a consequence of disappearance of the activation barrier for electron transfer. In addition to the Robin−Day classification, a number of recent studies have reported complicated systems exhibiting an intermediate behavior between class II and class III which are now categorized as borderline class II−III.[1a,c,d]

To investigate the extent of the electronic interaction between two redox centers, an absorption in the visible or near-infrared region is of prime importance as a systematic marker. Although class I mixed-valence compounds show no absorption, class II compounds generally exhibit a broad and weak absorption, called an IVCT (intervalence charge transfer) band, which originates from a light-driven process from one redox site to the other (from Ru^{II} to Ru^{III}, for example). In contrast, class III mixed-valence compounds show a narrow and intense absorption, which is traditionally called an IVCT band too, but arises from a transition between delocalized electronic levels and not from intramolecular charge transfer. Analysis of the IVCT bands by Marcus−Hush theory gives parameters that define the thermal electron transfer barrier.[4]

One of the continuing themes is preparation of mixed-valence assemblies containing multiple redox centers, which has significant implications in understanding long-range electron transfer in biological systems, as well as in designing molecular conductive devices.[1f,5] A redox-active mononuclear transition-metal

Received: February 23, 2011
Published: May 10, 2011

dx.doi.org/10.1021/ja2016813 | J. Am. Chem. Soc. 2011, 133, 8307–8316

Chart 1. Symmetrical Salen Ligands and Their Abbreviations

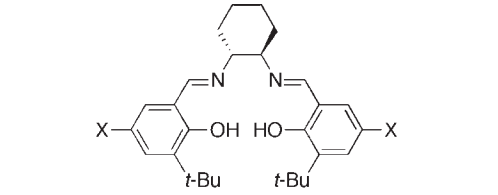

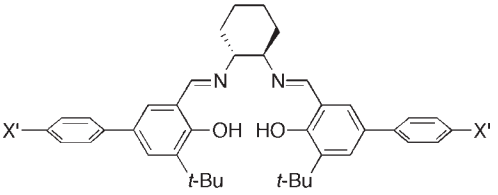

Chart 2. Nonsymmetrical Salen Ligands and Their Abbreviations

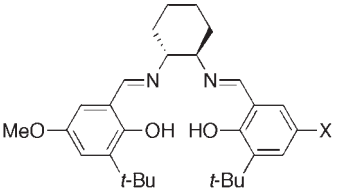

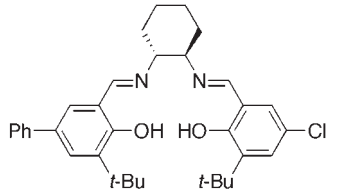

center (M) carrying two redox-active ligands (L) generates a mixed-valence system, L−M−$L^{\bullet+}$, upon one-electron oxidation. In this system, the $L^{\bullet+}$ moiety as an electron acceptor is electronically linked to the remote L moiety as an electron donor via a neighboring redox-active metal ion, providing an opportunity to study the nature of electron transfer from L to $L^{\bullet+}$ mediated by a redox-active metal ion as a bridge. Examples of such systems include transition-metal complexes with dioxolenes,[6] *o*-phenylenediamines,[7] benzene-1,2-dithiolates,[8] *o*-iminophenolate,[9] α-iminopyridines,[10] and salens.[11] To clarify electronic communications among multiple redox centers, the most important issue is to precisely assign visible and near-infrared absorptions, which would possibly contain at least two overlapping transitions, IVCT from L to $L^{\bullet+}$ and MLCT (metal-to-ligand charge transfer) from M to $L^{\bullet+}$. However, it has been a very difficult task to address this issue, and theoretical calculations have been frequently employed as the only available tool in previous studies.[12]

We herein report mixed-valence ligand radicals from manganese(III) salen complexes. To investigate redox matching between a manganese(III) center and phenolate ligands, we prepared salen ligands with different redox potentials by varying the substituent as shown in Chart 1. We have been interested in active species that are transiently generated from chiral manganese(III) salen complexes, which are well-known as the most excellent asymmetric oxidation catalyst.[13] During the course of the studies,[14] we have already reported a manganese(III)−phenoxyl radical species with a sterically hindered salen ligand, although the mixed-valence property could not be studied due to inability to reliably assign IVCT transitions.[14b] The manganese(III)−phenoxyl radical species is shown to be readily converted to manganese(IV)−phenolate species via intramolecular electron transfer, suggesting the redox potential of the manganese(III) ion and the phenolate in salen complexes is very close. We thus believe the mixed-valence property of ligand radicals from manganese(III) salen complexes is of great interest. However, the close proximity of the redox levels accompanies the ambiguity on whether the locus of oxidation is metal-centered or ligand-centered, which is carefully investigated in the present study. Indeed, very few examples are known for manganese−phenoxyl radical complexes,[14b,15] in contrast to the abundance of high-valent manganese−phenolate complexes.[16]

The key point in the present study is precise assignment of the IVCT band from a phenolate to a phenoxyl radical by use of nonsymmetrical phenoxyl radicals bearing the phenolate with different electron-donor abilities (Chart 2). The present study unambiguously shows that a d^4 high-spin manganese(III) ion forms a class II mixed-valence system between the *localized* phenoxyl radical and the phenolate, which is in clear contrast to the *delocalized* class III radical over the two phenolate rings for a d^8 low-spin nickel(II) ion with the same salen ligand, as reported by other groups.[11h,j] It is also shown that the redox potential of the salen ligand modulates the electron transfer from the phenolate to the phenoxyl radical with the nickel(II) ion as a mediator.

RESULTS AND DISCUSSION

Synthesis, Characterization, and One-Electron Oxidation of Electronically Diverse Mn^{III}(salen)(OTf) and Ni^{II}(salen). Symmetrical and nonsymmetrical salen ligands utilized in this study are abbreviated in this paper as shown in Charts 1 and 2, respectively. Manganese(III) salen complexes are synthesized using triflate as a counterion. We confirmed that nonsymmetrical salen complexes do not isomerize to two symmetrical salen complexes in solution using ESI-MS (electrospray ionization mass spectrometry) (Figures S1 and S2, Supporting Information). Cyclic voltammetry measurements were carried out at 233 K in CH_2Cl_2 containing 0.1 M Bu_4NOTf (Figures S3−S6, Supporting Information), and the electrochemical parameters referenced versus the ferrocenium/ferrocene couple (Fc^+/Fc) are summarized in Table 1. The first redox potential ($E_{1/2}{}^1$) of manganese(III) salen complexes is increased in the order MeO (0.46 V) ≪ Ph (0.68 V) < *t*-Bu (0.70 V) ≪ Cl (0.86 V) as a substituent on the phenolate ring. The same trend is observed for nickel(II) salen complexes, which exhibit an increased $E_{1/2}{}^1$ value in the order MeO (0.21 V) < *t*-Bu (0.36 V) < Cl (0.49 V). Accordingly, upon one-electron oxidation of nonsymmetrical salen complexes prepared in this study, one of the two phenolates is preferentially oxidized in all the cases. Table 1 includes $\Delta E_{1/2}$ ($= E_{1/2}{}^2 - E_{1/2}{}^1$) values, which have been used for the assessment of the extent of the electronic interaction between two redox sites.[1f]

One-electron-oxidized products are generated by controlled-potential electrochemical oxidation at 203 K in CH_2Cl_2 containing 0.1 M Bu_4NOTf in a thin-layer quartz cell for UV−vis−NIR absorption measurements. We carefully applied a voltage which

dx.doi.org/10.1021/ja2016813 |*J. Am. Chem. Soc.* 2011, 133, 8307–8316

Table 1. Electrochemical Parameters (V) Measured in CH_2Cl_2 Containing 0.1 M Bu_4NOTf at 233 K[a]

	E_a^1	E_a^2	E_c^1	E_c^2	$E_{1/2}^1$	$E_{1/2}^2$	$\Delta E_{1/2}$
Mn^{III}(L-OMe)	0.51	0.80	0.41	[b]	0.46		
Mn^{III}(L-*t*-Bu)	0.75	1.10	0.64	0.97	0.70	1.04	0.34
Mn^{III}(L-Ph)	0.72	1.00	0.63	0.90	0.68	0.95	0.27
Mn^{III}(L-Cl)	0.91	1.14	0.81	1.03	0.86	1.09	0.23
Mn^{III}(L-Ph-*p*-OMe)	0.58	0.74	0.47	[b]	0.53		
Mn^{III}(L-OMe/*t*-Bu)	0.52	[c]	0.42	[b]	0.47		
Mn^{III}(L-OMe/Cl)	0.56	1.09	0.44	[b]	0.50		
Mn^{III}(L-Ph/Cl)	0.75	1.27	0.65	[b]	0.70		
Ni^{II}(L-OMe)	0.26	[d]	0.16	[b]	0.21		
Ni^{II}(L-*t*-Bu)	0.42	0.79	0.30	0.66	0.36	0.73	0.37
Ni^{II}(L-Cl)	0.64	0.82	0.33	0.49	0.49	0.66	0.17
Ni^{II}(L-OMe/*t*-Bu)	0.28	0.73	0.17	[b]	0.23		
Ni^{II}(L-OMe/Cl)	0.31	0.79	0.21	[b]	0.26		

[a] E_a^1 and E_a^2 are the first and second anodic oxidation peak potentials, respectively, and E_c^1 and E_c^2 are the first and second cathodic reduction peak potentials, respectively. $E_{1/2}^1$ values are calculated as averaged values of E_a^1 and E_c^1, and $E_{1/2}^2$ values are calculated as averaged values of E_a^2 and E_c^2. $\Delta E_{1/2}$ values are defined as $E_{1/2}^2 - E_{1/2}^1$. Potentials are referenced versus the ferrocenium/ferrocene couple. Potentials are determined with cyclic voltammetry (Figure S3−S6, Supporting Information). [b] Corresponding peaks are not observed. [c] Two peaks at 0.95 and 1.10 V are observed. [d] Two peaks at 0.58 and 0.69 V are observed.

is higher than the first anodic oxidation peak (E_a^1) but is lower than the second anodic oxidation peak (E_a^2) to obtain one-electron-oxidized products selectively. We monitored UV−vis spectral changes during electrochemical oxidations and checked the presence of isosbestic points as a measure for the purity of one-electron-oxidized products (Figures S7−S10, Supporting Information). We also confirmed the starting complex is regenerated with clear isosbestic points upon the electrochemical reduction. It was shown that one-electron-oxidized products are cleanly generated from all the manganese(III) and nickel(II) salen complexes except for Mn^{III}(L-Cl). One-electron-oxidized products from manganese(III) salen complexes are alternatively synthesized according to the procedure shown in Scheme 1. The SbF_6^- counterion is the only choice for the isolation of analytically pure solid samples among other counterions such as TfO^-, BF_4^-, and PF_6^-. It was confirmed that the isolated Mn(salen)$(SbF_6)_2$ samples that are dissolved in CH_2Cl_2 containing 0.1 M Bu_4NOTf exhibit UV−vis spectra identical to those of the electrochemically generated samples. One-electron-oxidized products from nickel(II) salen complexes are alternatively synthesized and isolated with SbF_6^- as a counterion, according to the procedure reported by Storr and Stack.[11h]

Evidence for Manganese(III)−Phenoxyl Radical. Figure 1 shows ^1H and ^2H NMR spectra of Mn(salen)$(SbF_6)_2$ from Mn^{III}(L-*t*-Bu) and Mn^{III}(L-*t*-Bu-d_4) (Chart 3). In L-*t*-Bu-d_4, ^2H atoms are selectively incorporated into the phenolate rings (80% D) and the *tert*-butyl groups (7% D).[14d] Plots of chemical shifts versus $1/T$ in the range from 193 to 253 K are linear with intercepts ($1/T$ = 0) in the diamagnetic region (Figure S11, Supporting Information). The ^1H NMR signals of high intensity at −3.6 and −22.0 ppm are unambiguously assigned as arising from the *tert*-butyl groups, in comparison with the ^2H NMR spectrum. In the case of the crystallographically characterized Mn^{IV}(salen)$(L)_2$ complexes (L = CF_3CH_2O, N_3, and Cl), the ^1H

Scheme 1. Preparation of One-Electron-Oxidized Manganese(III) Salen Complexes

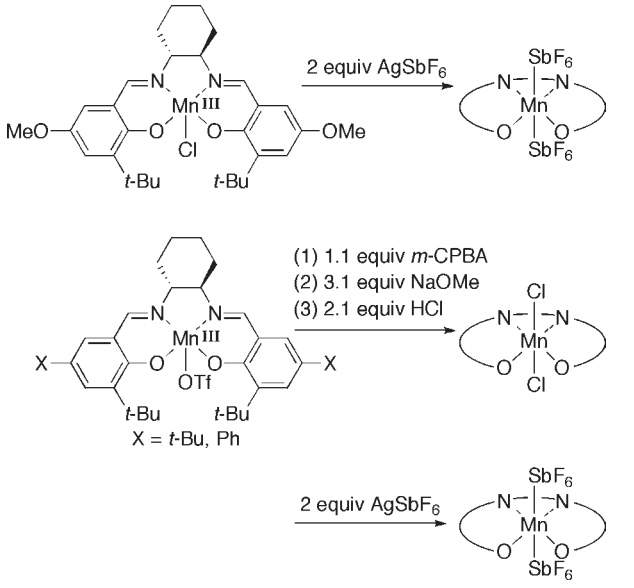

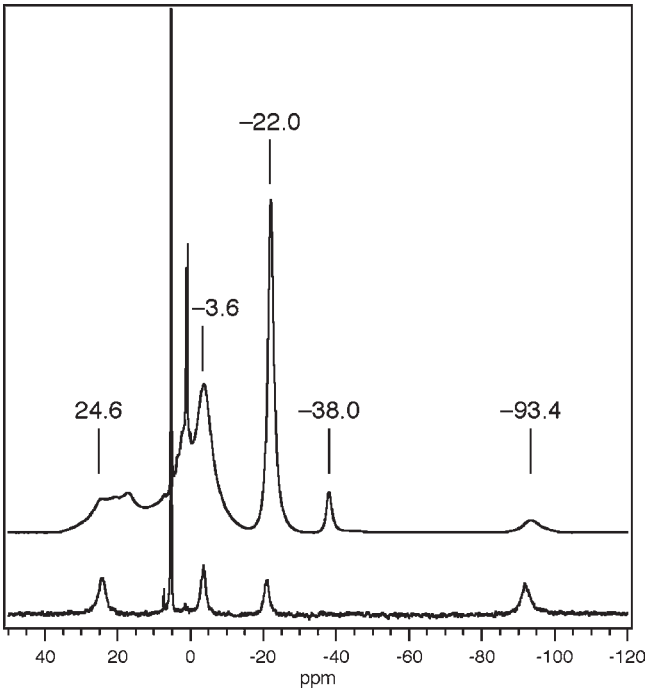

Figure 1. ^1H NMR spectrum of a 20 mM solution of $Mn^{III}(salen^{\bullet+})(SbF_6)_2$ from Mn^{III}(L-*t*-Bu) in CD_2Cl_2 at 233 K (top) and ^2H NMR spectrum of a 5 mM solution of $Mn^{III}(salen^{\bullet+})(SbF_6)_2$ from Mn^{III}(L-*t*-Bu-d_4) in CH_2Cl_2 at 233 K (bottom).

NMR signals of the *tert*-butyl groups appear within the diamagnetic region (2.6−4.8 ppm), indicative of a negligibly small dipolar interaction between the manganese center and the *tert*-butyl groups.[14d] Therefore, the significant paramagnetic shift of the *tert*-butyl groups in Mn(salen)$(SbF_6)_2$ clearly indicates the presence of an unpaired electron on the phenolate rings in close vicinity to the *tert*-butyl groups. Then the Mn(salen)$(SbF_6)_2$

dx.doi.org/10.1021/ja2016813 |J. Am. Chem. Soc. 2011, 133, 8307–8316

Chart 3

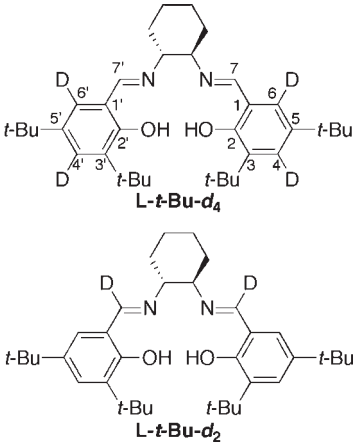

complex is a salen ligand radical complex, $Mn^{III}(salen^{\bullet+})(SbF_6)_2$. Interestingly, the ^1H and ^2H NMR signal that arises from 4/4′-H or 6/6′-H of the phenolate rings appears at −19 to −24 ppm in $Mn^{IV}(salen)(L)_2$ (L = CF_3CH_2O, N_3, and Cl),[14d] while the corresponding signal is largely shifted to −93.4 ppm in $Mn^{III}(salen^{\bullet+})(SbF_6)_2$, which could be utilized as a diagnosis for the formation of the salen ligand radical.

We then focused on the ^2H NMR signal at the 7/7′ position of the azomethine group as a probe to investigate electronic structures and prepared Mn^{III}(L-*t*-Bu-d_2) (Chart 3), which is selectively deuterated at the 7/7′ position (99.5% D). As shown in Figure 2a, the $Mn^{III}(salen^{\bullet+})(SbF_6)_2$ complex shows a 7/7′-D NMR signal at −514 ppm, which is more shifted as compared to that of $Mn^{IV}(salen)(N_3)_2$ (−370 ppm), but is less shifted than that of Mn^{III}(salen)(OTf) (−574 ppm). Plots of chemical shifts versus $1/T$ are linear with intercepts ($1/T = 0$) in the diamagnetic region in the case of $Mn^{IV}(salen)(N_3)_2$ and Mn^{III}(salen)(OTf), but in the case of $Mn^{III}(salen^{\bullet+})(SbF_6)_2$, the intercept is considerably deviated from the diamagnetic region. The nonzero intercept of the Curie plot might be due to a thermally accessible excited state.

We then prepared one-electron-oxidized products from Mn^{III}(L-OMe) and Mn^{III}(L-Ph), to investigate the effect of the substituent on the phenolate rings. Figure 3 shows ^1H NMR spectra of isolated Mn(salen)$(SbF_6)_2$ complexes from Mn^{III}(L-OMe), Mn^{III}(L-*t*-Bu), and Mn^{III}(L-Ph) at 253 K, a higher temperature than that employed in Figure 1 due to broadening of a signal. ^1H NMR signals for one of the phenolate protons appear at −105, −85, and −54 ppm in Mn(salen)$(SbF_6)_2$ complexes from Mn^{III}(L-OMe), Mn^{III}(L-*t*-Bu), and Mn^{III}(L-Ph), respectively. The ^1H NMR signal for the phenolate protons in Mn(salen)$(SbF_6)_2$ from Mn^{III}(L-Ph) is least shifted (−54 ppm), but is still more shifted than the corresponding signal at −19.8 ppm in Mn^{IV}(salen)$(Cl)_2$ (Figure S12, Supporting Information). Then it is indicated that one-electron oxidation of Mn^{III}(L-OMe) and Mn^{III}(L-Ph) in the presence of a weakly bound counterion such as TfO^- and SbF_6^- also generates a $Mn^{III}(salen^{\bullet+})$ complex. Additional evidence for the assignment as $Mn^{III}(salen^{\bullet+})$ comes from near-infrared absorptions that are reliably assigned as arising from the charge transfer transition from the phenolate to the phenoxyl radical (vide infra). We then compare EPR spectra of isolated $Mn^{III}(salen^{\bullet+})(SbF_6)_2$ complexes dissolved in CH_2Cl_2 containing 1.0 M Bu_4NOTf (Figure 4). The resulting $Mn(salen^{\bullet+})(OTf)_2$

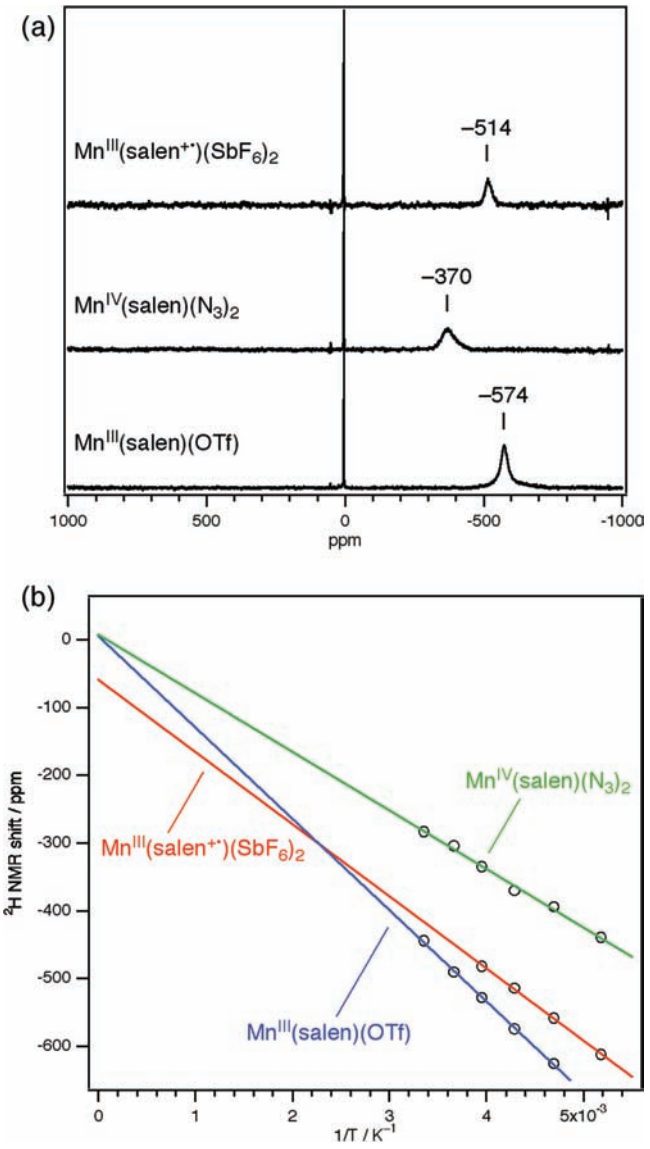

Figure 2. (a) ^2H NMR spectra of a 20 mM solution of $Mn^{III}(salen^{\bullet+})(SbF_6)_2$ (top), a 40 mM solution of $Mn^{IV}(salen)(N_3)_2$ (middle), and a 40 mM solution of Mn^{III}(salen)(OTf) (bottom) from Mn^{III}(L-*t*-Bu-d_2) in CH_2Cl_2 at 233 K. (b) ^2H NMR Curie plots and linear least-squares fits to the data for $Mn^{III}(salen^{\bullet+})(SbF_6)_2$ (red line), $Mn^{IV}(salen)(N_3)_2$ (green line), and Mn^{III}(salen)(OTf) (blue line) from Mn^{III}(L-*t*-Bu-d_2).

complexes derived from Mn^{III}(L-OMe), Mn^{III}(L-*t*-Bu), and Mn^{III}(L-Ph) commonly exhibit a weak signal at $g = 5.3-5.7$ and a broad signal at $g = 2.0$. The signals at $g = 5.3-5.7$ display a six-line hyperfine splitting due to the $I = 5/2$ ^{55}Mn nucleus. Sharp signals marked with an asterisk may arise from a free ligand radical that is not coupled with a manganese(III) ion. A set of broad $g \approx 2$ and $g \approx 5$ signals are assigned as a rhombic $S = 3/2$ system ($E/D \approx 0.30$), which is consistent with the magnetic susceptibility data for $Mn^{III}(salen^{\bullet+})(SbF_6)_2$ from Mn^{III}(L-*t*-Bu) (Curie constant $C = 1.95$ cm^3 mol^{-1} K, axial zero-field-spitting parameter $|D| = 2.2$ cm^{-1}, Figure 5). The $S = 3/2$ system observed for $Mn^{III}(salen^{\bullet+})(SbF_6)_2$ would be accounted for by an antiferromagnetic coupling between the manganese(III) ion ($S = 4/2$) and the phenoxyl radical ($S = 1/2$). Close inspection of the $\chi_m T$ versus T

dx.doi.org/10.1021/ja2016813 |J. Am. Chem. Soc. 2011, 133, 8307–8316

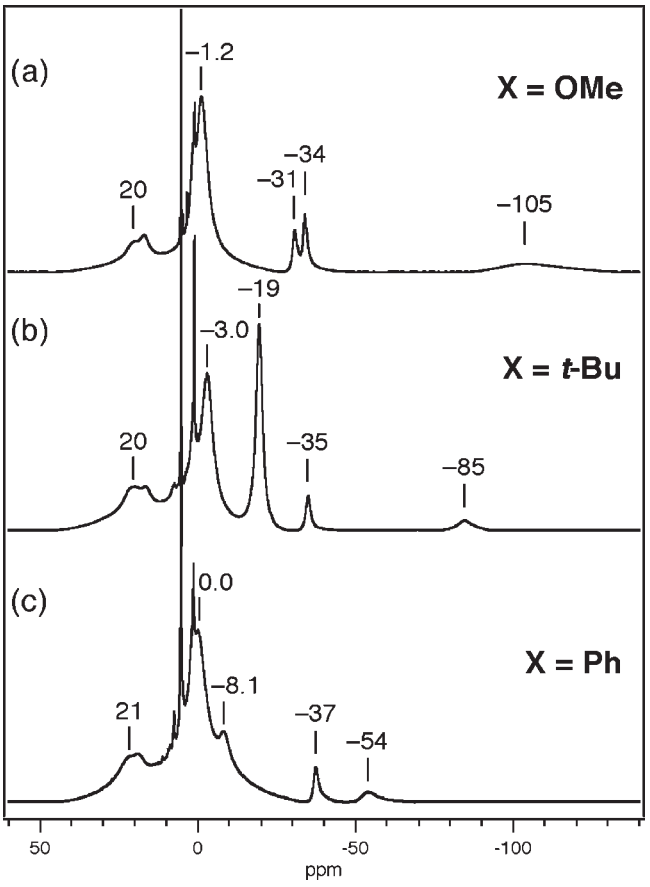

Figure 3. ^{1}H NMR spectra of $Mn^{III}(salen^{\bullet+})(SbF_6)_2$ derived from (a) Mn^{III}(L-OMe) (30 mM), (b) Mn^{III}(L-*t*-Bu) (20 mM), and (c) Mn^{III}(L-Ph) (10 mM) in CD_2Cl_2 at 253 K.

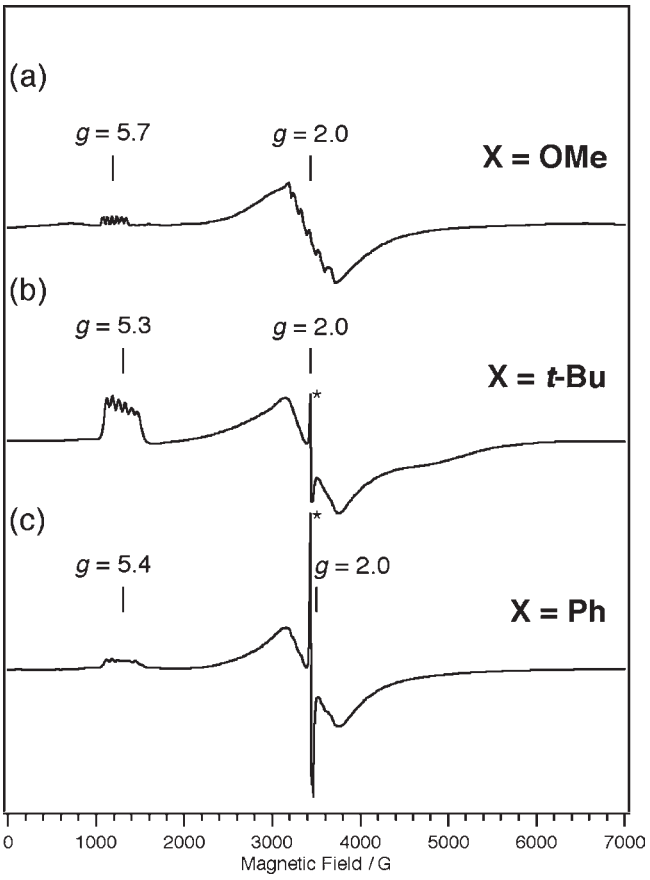

Figure 4. X-band EPR spectra of a 10 mM frozen solution of $Mn^{III}(salen^{\bullet+})(SbF_6)_2$ derived from (a) Mn^{III}(L-OMe), (b) Mn^{III}(L-*t*-Bu), and (c) Mn^{III}(L-Ph). Conditions: temperature, 4 K; solvent, frozen CH_2Cl_2 containing 1 M Bu_4NOTf; microwave frequency, 9.65 GHz; microwave power, 0.5 mW; modulation amplitude, 7 G; time constant, 163.84 ms; conversion time, 163.84 ms.

plot shows a slight upward deviation from the theoretical line at higher temperature (>250 K), which is in accord with the nonzero intercept of the Curie plot for the ^{2}H NMR signal. It is noted that the $S = 3/2$ spin system is a common feature with the $Mn^{IV}(salen)(L)_2$ complexes (L = CF_3CH_2O, N_3, Cl, and NO_3), as shown by their EPR spectra[14d] and magnetic susceptibility data (Figure S13, Supporting Information).

Ligand Radicals from Manganese(III) Salen Complexes as Class II Mixed-Valence Compounds. As shown in Figure 6, the $Mn^{III}(salen^{\bullet+})(OTf)_2$ complexes from Mn^{III}(L-OMe), Mn^{III}(L-*t*-Bu), and Mn^{III}(L-Ph) exhibit intense absorptions at 455, 435, and 377 nm, respectively, which could be assigned as $\pi-\pi^*$ transitions of the coordinated phenoxyl radical.[17] The most important point in defining a mixed-valence property is an absorption feature in the visible and near-infrared regions. Indeed, the $Mn^{III}(salen^{\bullet+})(OTf)_2$ complexes from Mn^{III}(L-OMe), Mn^{III}(L-*t*-Bu), and Mn^{III}(L-Ph) commonly exhibit characteristic broad absorptions of similarly low intensity in the near-infrared region (λ_{max} = 1270, 1480, and 1510 nm, respectively). It is also interesting to note that the $Mn^{III}(salen^{\bullet+})(OTf)_2$ complex from Mn^{III}(L-Ph) exhibits an additional intense absorption in the visible region (λ_{max} = 650 nm).

To unambiguously assign these absorptions, we compare the absorption spectra of $Mn^{III}(salen^{\bullet+})(OTf)_2$ from symmetrical Mn^{III}(L-OMe) with nonsymmetrical Mn^{III}(L-OMe/*t*-Bu) and Mn^{III}(L-OMe/Cl) (Figure 7). The $Mn^{III}(salen^{\bullet+})(OTf)_2$ complex from Mn^{III}(L-OMe) exhibits a broad absorption of low intensity in the near-infrared region at 1270 nm (ε = 1400 M^{-1} cm^{-1}), as shown in Figure 6a. Quite interestingly, the $Mn^{III}(salen^{\bullet+})(OTf)_2$ complexes from nonsymmetrical Mn^{III}(L-OMe/*t*-Bu) and Mn^{III}(L-OMe/Cl), in which one of the MeO groups in Mn^{III}(L-OMe) is replaced by *t*-Bu and Cl, show broad absorptions of similarly low intensity at 1015 nm (ε = 1100 M^{-1} cm^{-1}) and 890 nm (ε = 1200 M^{-1} cm^{-1}), respectively (Figure 7). The absorptions shifted to a higher energy are consistent with the assignment as a charge transfer band from the phenolate to the phenoxyl radical, because an excitation energy required for photoinduced intramolecular electron transfer would increase in the order L-OMe < L-OMe/*t*-Bu < L-OMe/Cl (Scheme 2), as deduced from the redox potentials of Mn^{III}(L-OMe) (0.46 V), Mn^{III}(L-*t*-Bu) (0.70 V), and Mn^{III}(L-Cl) (0.86 V) (Table 1). It is noted that the ligand-to-ligand charge transfer depicted in Scheme 2 is exactly the IVCT band from a localized Robin−Day class II mixed-valence system, and then the $Mn^{III}(salen^{\bullet+})(OTf)_2$ complex from Mn^{III}(L-OMe) is unambiguously assigned as a class II mixed-valence compound.

The $Mn^{III}(salen^{\bullet+})(OTf)_2$ complex from Mn^{III}(L-Ph) bearing Ph as a substituent exhibits an additional intense absorption in the visible region at 650 nm (Figure 6c), which is another point to be clarified in defining the mixed-valence property of $Mn^{III}(salen^{\bullet+})(OTf)_2$. We then compare the absorption spectra of

dx.doi.org/10.1021/ja2016813 |J. Am. Chem. Soc. 2011, 133, 8307–8316

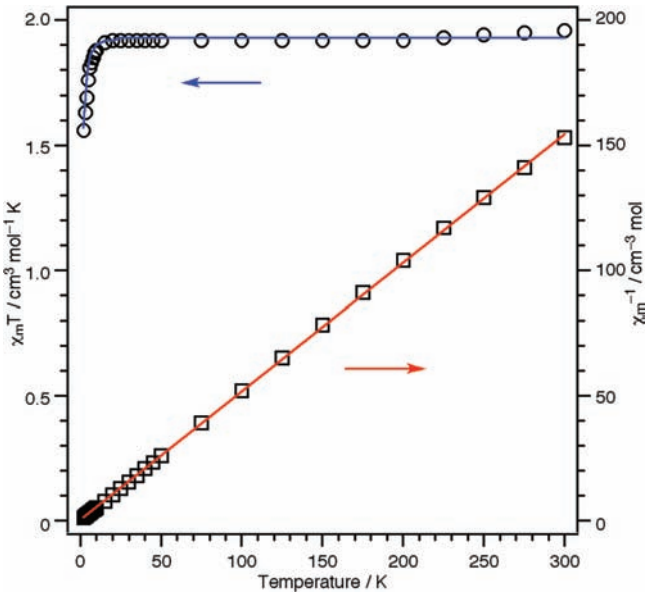

Figure 5. $\chi_m T$ (○) and χ_m^{-1} (□) for a polycrystalline sample of $Mn^{III}(salen^{\bullet+})(SbF_6)_2$ from Mn^{III}(L-*t*-Bu) as a function of temperature T in an applied field of 1 kOe. The χ_m^{-1} vs T plots (>30 K) were analyzed by the Curie–Weiss law $1/\chi_m = (1/C)T - \Theta/C$ with C = 1.95 $cm^3\ mol^{-1}$ K and $\Theta = -1.21$ K (red line). The $\chi_m T$ vs T plots were simulated by julX written by E. Bill with $E/D = 0.30$, $D = 2.2\ cm^{-1}$, and $g = 2.00$ (blue line). For details regarding julX, see http://ewww.mpi-muelheim.mpg.de/bac/logins/bill/julX_en.php.

$Mn^{III}(salen^{\bullet+})(OTf)_2$ from Mn^{III}(L-Ph) and nonsymmetrical Mn^{III}(L-Ph/Cl) (Figures 6c and 8a). The position of the absorption at 650 nm is not altered at all. This clearly indicates the intense absorption in the visible region at 650 nm cannot be an IVCT band between the phenolate and the phenoxyl radical, but is assigned as arising from the substructure containing the phenoxyl radical and the manganese(III) ion. To further investigate the origin of this absorption, we prepared the Mn^{III}(L-Ph-*p*-OMe) complex bearing *p*-methoxyphenyl groups instead of phenyl groups. The $Mn^{III}(salen^{\bullet+})(OTf)_2$ complex from Mn^{III}(L-Ph-*p*-OMe) exhibits an intense absorption at 810 nm (Figure 8b). The shift to a lower energy suggests that this absorption arises from a charge transfer from the aromatic substituent on the phenolate rings to the phenoxyl radical. We already reported that the $Mn^{III}(salen^{\bullet+})(OTf)_2$ complex from the sterically hindered manganese(III) salen complex bearing mesityl groups exhibits intense absorptions around 900 nm,[14b] which is now most probably assigned as a charge transfer from the mesityl groups to the phenoxyl radical. It is interesting to note that the near-infrared broad absorption at 1510 nm in $Mn^{III}(salen^{\bullet+})(OTf)_2$ from Mn^{III}(L-Ph) is shifted to 1070 nm in $Mn^{III}(salen^{\bullet+})(OTf)_2$ from nonsymmetrical Mn^{III}(L-Ph/Cl) (Figures 6c and 8a), which clearly indicates that this absorption arises from a charge transfer from the phenolate to the phenoxyl radical. Thus, the ligand radicals from the manganese(III) salen complexes bearing aromatic substituents also belong to Robin–Day class II.

The corresponding ligand-to-ligand charge transfer band in $Mn^{III}(salen^{\bullet+})(OTf)_2$ from Mn^{III}(L-*t*-Bu) appears at 1480 nm (ε = 1600 $M^{-1}\ cm^{-1}$), which is almost the same wavelength as that observed for $Mn^{III}(salen^{\bullet+})(OTf)_2$ from Mn^{III}(L-Ph) (Figure 6b,c). This is in agreement with the nearly identical redox potentials for Mn^{III}(L-*t*-Bu) and Mn^{III}(L-Ph) (Table 1).

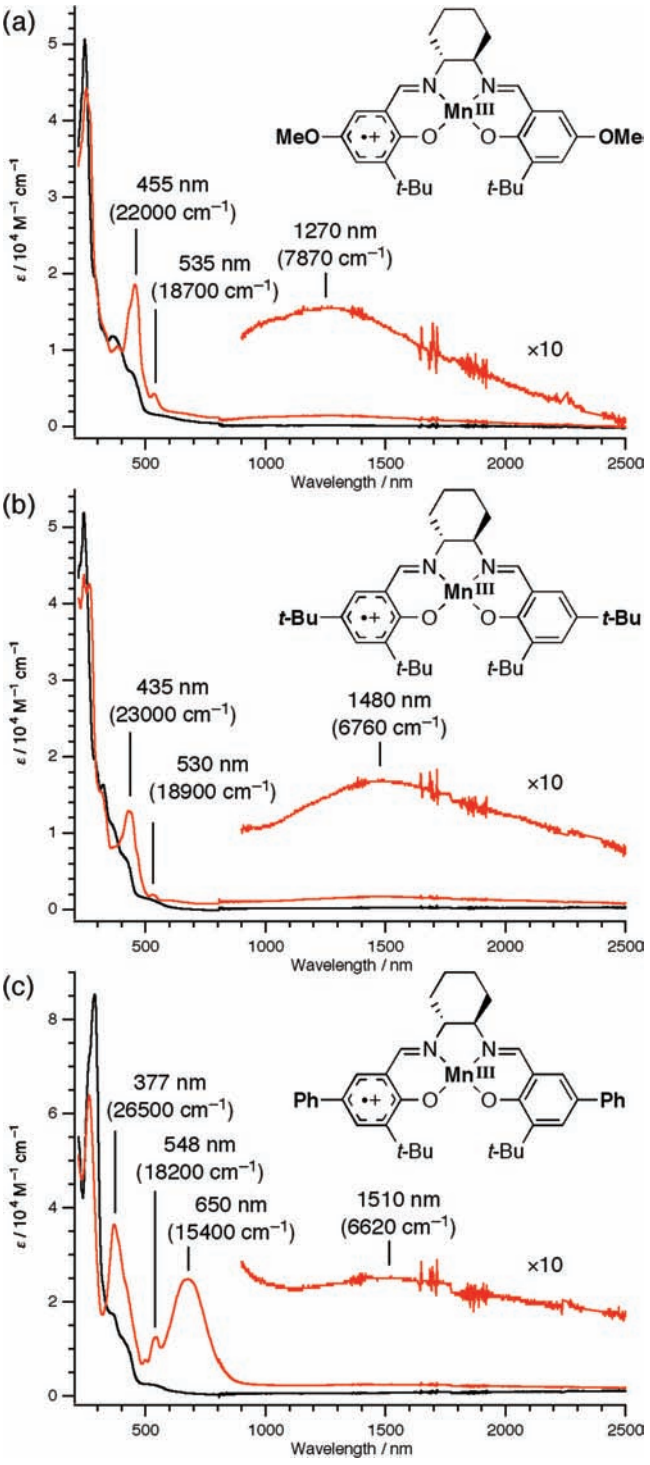

Figure 6. Absorption spectra of one-electron-oxidized products (red line) that are generated electrochemically from (a) Mn^{III}(L-OMe) (0.8 mM), (b) Mn^{III}(L-*t*-Bu) (0.8 mM), and (c) Mn^{III}(L-Ph) (0.4 mM) (black line) at 203 K. Data in the 2230–2260 and 2330–2400 nm ranges were deleted due to intense noises derived from the absorption of the solvent.

In the case of the Mn^{III}(L-OMe) complex, which shows a lower oxidation potential by 0.20 V than Mn^{III}(L-*t*-Bu) and Mn^{III}(L-Ph) (Table 1), the ligand-to-ligand absorption in $Mn^{III}(salen^{\bullet+})(OTf)_2$ is shifted to higher energy at 1270 nm (Figure 6a).

dx.doi.org/10.1021/ja2016813 |*J. Am. Chem. Soc.* 2011, 133, 8307–8316

We also carried out Marcus−Hush analysis of the IVCT bands. According to the Marcus−Hush theory, the bandwidth at half-height ($\Delta\nu_{1/2}$, cm^{-1}) for the IVCT transition from a class II mixed-valence system is predicted by the following equation:

$$\Delta\nu_{1/2} = \sqrt{16RT(\ln 2)\nu_{max}} \quad (1)$$

where R is the gas constant, T is the temperature (K), and ν_{max} is the band maximum (cm^{-1}). When the experimental $\Delta\nu_{1/2}$ value is equal to or broader than the theoretical value, the electronic structure is regarded as class II. When the experimental $\Delta\nu_{1/2}$ value is significantly smaller than the theoretical value, the mixed-valence system is assigned as class III or borderline class II−III. The near-infrared absorptions that are commonly observed for $Mn^{III}(salen^{\bullet+})$ prepared in this study are consistent with the assignment as class II IVCT bands: for $[Mn^{III}(L\text{-}OMe)]^+$, $\Delta\nu_{1/2}$(theoretical) = 3500 cm^{-1} versus $\Delta\nu_{1/2}$(experimental) = 4600 cm^{-1}, for $[Mn^{III}(L\text{-}t\text{-}Bu)]^+$, $\Delta\nu_{1/2}$(theoretical) = 3300 cm^{-1} versus $\Delta\nu_{1/2}$(experimental) = 5300 cm^{-1}, and for $[Mn^{III}(L\text{-}Ph)]^+$, $\Delta\nu_{1/2}$(theoretical) = 3200 cm^{-1} versus

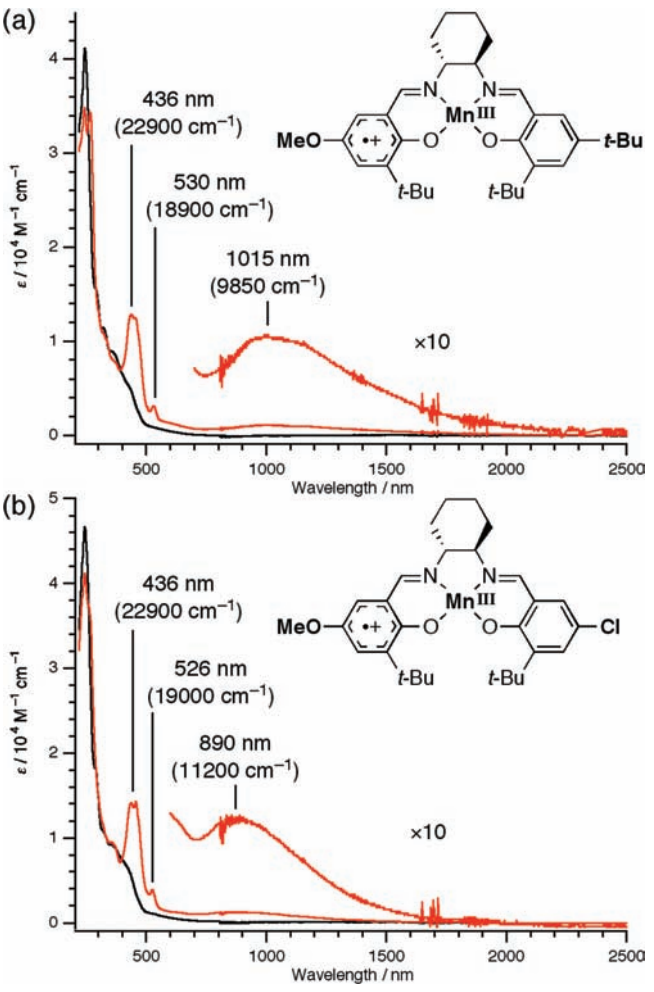

Figure 7. Absorption spectra of one-electron-oxidized products (red line) that are generated electrochemically from (a) Mn^{III}(L-OMe/*t*-Bu) (0.8 mM) and (b) Mn^{III}(L-OMe/Cl) (0.8 mM) (black line) at 203 K. Data in the 2230−2260 and 2330−2400 nm ranges were deleted due to intense noises derived from the absorption of the solvent.

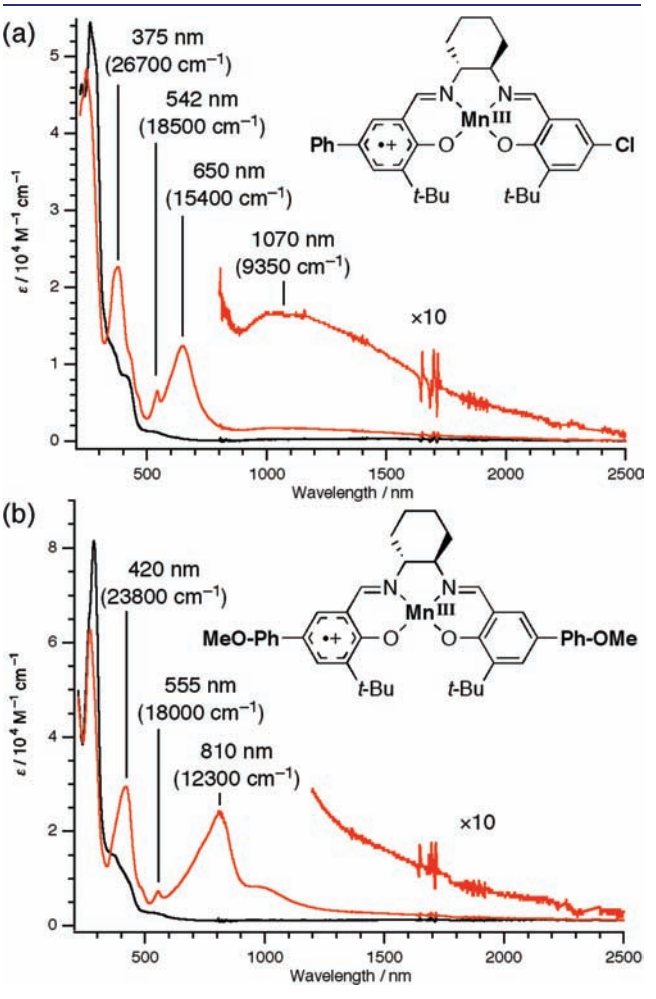

Figure 8. Absorption spectra of one-electron-oxidized products (red line) that are generated electrochemically from (a) Mn^{III}(L-Ph/Cl) (0.8 mM) and (b) Mn^{III}(L-Ph-*p*-OMe) (0.4 mM) (black line) at 203 K. Data in the 2230−2260 and 2330−2400 nm ranges were deleted due to intense noises derived from the absorption of the solvent.

Scheme 2

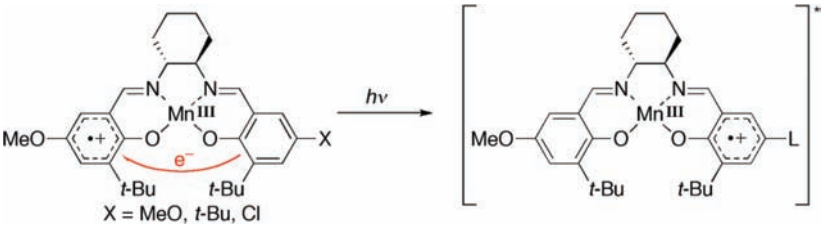

dx.doi.org/10.1021/ja2016813 |*J. Am. Chem. Soc.* 2011, 133, 8307–8316

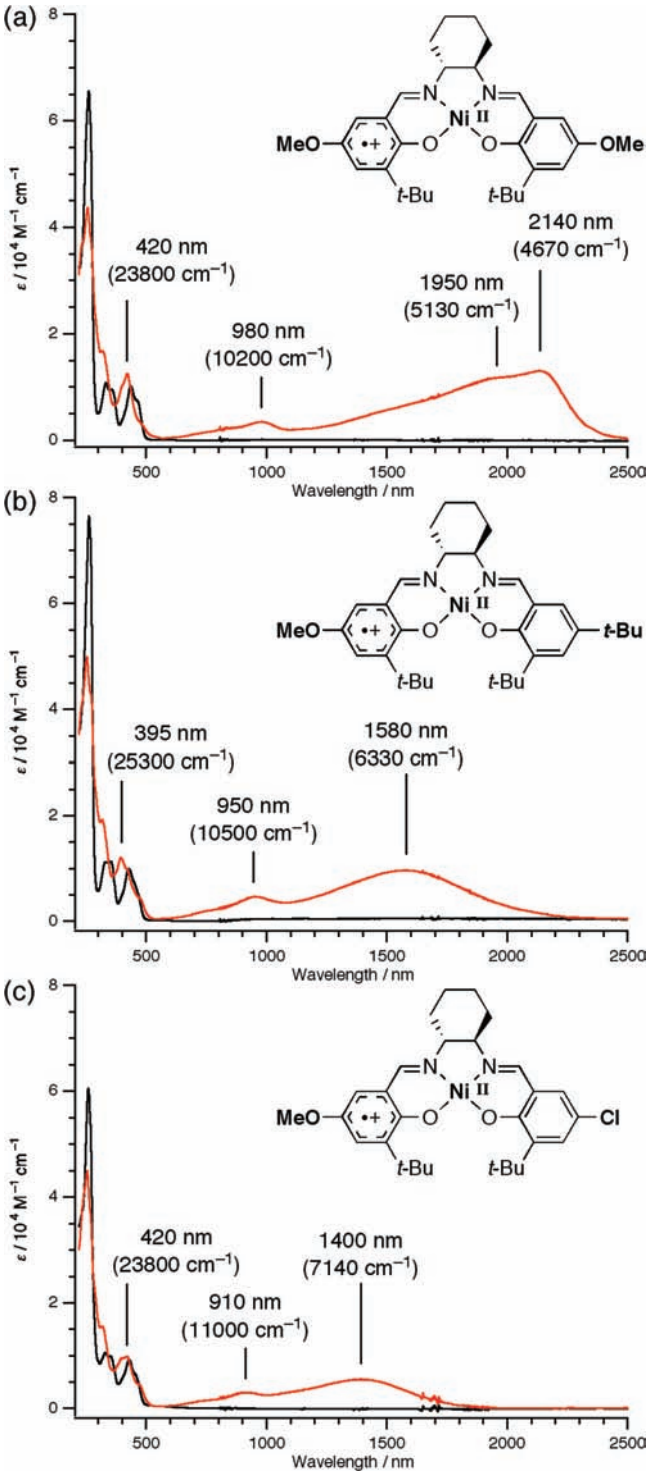

Figure 9. Absorption spectra of a 0.5 mM solution of one-electron-oxidized products (red line) that are generated electrochemically from (a) Ni^{II}(L-OMe), (b) Ni^{II}(L-OMe/*t*-Bu), and (c) Ni^{II}(L-OMe/Cl) (black line) at 203 K. Data in the 2230−2260 and 2330−2400 nm ranges were deleted due to intense noises derived from the absorption of the solvent.

$\Delta\nu_{1/2}$(experimental) = 5700 cm^{-1}. It is thus concluded that a manganese(III) ion forms a Robin−Day class II mixed-valence system between the phenoxyl radical and the phenolate. We recently reported a quantum chemical calculation for Mn^{IV}(salen)(OH) and Mn^{III}(salen$^{\bullet+}$)(OH_2) using B3LYP density functional methods.[14e] The calculation nicely reproduces an electronic structural change from manganese(IV)−phenolate to manganese(III)−phenoxyl radical upon the exchange of the external axial ligand, but in the geometry-optimized Mn^{III}(salen$^{\bullet+}$)(OH_2), the two phenolate rings are structurally identical, which is erroneously indicative of a fully delocalized class III ligand radical.

Transition from Class II to Class III Mixed-Valence Systems in Ligand Radicals from Nickel(II) Salen Complexes. Our methodology using a series of nonsymmetrical salen complexes is applied for the analysis of the Ni^{II}(salen$^{\bullet+}$) complex from Ni^{II}(L-*t*-Bu), which was previously shown to be a fully delocalized Robin−Day class III mixed-valence compound by Shimazaki, Storr, and Stack.[11h,j] One of the best pieces of evidence for this assignment is an intense near-infrared absorption at 2130 nm ($\varepsilon = 2.15 \times 10^4\ M^{-1}\ cm^{-1}$). This near-infrared absorption is also observed for Ni^{II}(salen$^{\bullet+}$) that is alternatively prepared electrochemically from Ni^{II}(L-*t*-Bu) under the low-temperature conditions identical to those employed for the preparation of Mn^{III}(salen$^{\bullet+}$), although the absorption is slightly broadened (Figure S14, Supporting Information). The experimental $\Delta\nu_{1/2}$ value (790 cm^{-1}) estimated from this near-infrared absorption is 30% of the theoretical value (2700 cm^{-1}) obtained by eq 1, which is consistent with the assignment as a class III mixed-valence compound.

A new finding we have made herein is that the Ni^{II}(salen$^{\bullet+}$) complex from Ni^{II}(L-OMe) exhibits a significantly broad absorption in the range from 1200 to 2000 nm, in addition to a narrow absorption at 2140 nm, indicative of its different mixed-valence properties (Figure 9a). The narrow absorption at 2140 nm may be assigned as a delocalized class III IVCT band, in comparison with the absorption spectrum of Ni^{II}(salen$^{\bullet+}$) from Ni^{II}(L-*t*-Bu), a delocalized class III mixed-valence compound. This assignment is justified by complete disappearance of the narrow near-infrared absorption in the Ni^{II}(salen$^{\bullet+}$) complex from nonsymmetrical Ni^{II}(L-OMe/*t*-Bu) and Ni^{II}(L-OMe/Cl) (Figure 9b,c), in which the radical should be localized on the methoxyphenolate moiety due to the difference in the redox potential. In contrast, the broad absorption at ∼1950 nm in Ni^{II}(salen$^{\bullet+}$) from Ni^{II}(L-OMe), which is shifted to a higher energy (1580 and 1400 nm) in Ni^{II}(salen$^{\bullet+}$) from nonsymmetrical Ni^{II}(L-OMe/*t*-Bu) and Ni^{II}(L-OMe/Cl), is reliably assigned as a class II charge transfer transition of the type shown in Scheme 2. The band shape analysis by eq 1 is also consistent with the assignment as a class II IVCT ($\Delta\nu_{1/2}$(theoretical) = 2800 cm^{-1} versus $\Delta\nu_{1/2}$(experimental) = 2900 cm^{-1}). Then it is clearly shown that the Ni^{II}(salen$^{\bullet+}$) complex from Ni^{II}(L-OMe) is just on the transition between class II and class III mixed-valence compounds. Consistently, the Ni^{II}(salen$^{\bullet+}$) complex from Ni^{II}(L-OMe) shows an EPR signal (S = 1/2) at g = 2.023, which is close to the EPR signals at g = 2.021 and 2.016 for localized Ni^{II}(salen$^{\bullet+}$) from nonsymmetrical Ni^{II}(L-OMe/*t*-Bu) and Ni^{II}(L-OMe/Cl), as compared to the EPR signal at g = 2.045 for delocalized Ni^{II}(salen$^{\bullet+}$) from Ni^{II}(L-*t*-Bu) (Figure S15, Supporting Information). Very recently, Thomas and co-workers succeeded in the X-ray crystallographic analysis of the Ni^{II}(salen$^{\bullet+}$)(SbF_6) complex from Ni^{II}(L-OMe),[11k] which indeed shows a nonsymmetrical structure containing quinoid and phenolate rings, in contrast to a nearly 2-fold symmetric structure for Ni^{II}(salen$^{\bullet+}$)(SbF_6) from Ni^{II}(L-*t*-Bu), as reported by Storr and Stack.[11h]

dx.doi.org/10.1021/ja2016813 |*J. Am. Chem. Soc.* 2011, 133, 8307–8316

Chart 4

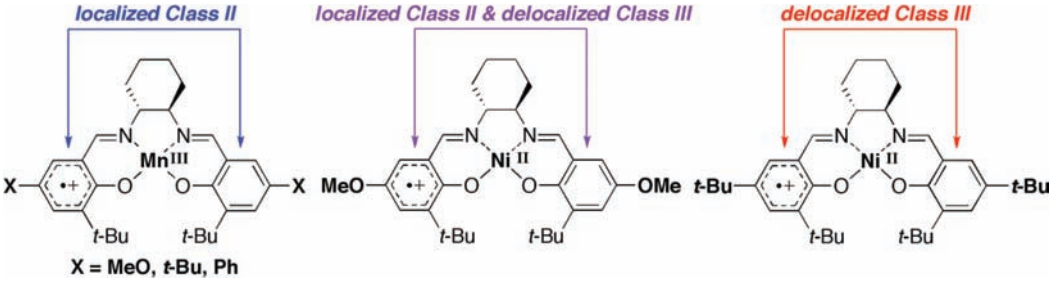

CONCLUSION

The present study unambiguously assigns IVCT and other transitions in ligand radicals from manganese(III) and nickel(II) salen complexes, which enables us to obtain otherwise inaccessible insight into electron transfer from the phenolate to the remote phenoxyl radical mediated by a neighboring metal ion. One of the most important findings is the function of the metal ion is strikingly different in mediating the electron transfer from the phenolate to the phenoxyl radical in metal salen complexes (Chart 4).[18] A d^4 high-spin manganese(III) ion forms a Robin–Day class II mixed-valence system, in which electron transfer is occurring between the *localized* phenoxyl radical and the phenolate. This is in clear contrast to a d^8 low-spin nickel(II) ion with the same salen ligand, which induces a *delocalized* radical (Robin–Day class III) over the two phenolate rings. The other point to be noted is a substituent effect on mixed-valence properties. In the case of the $Ni^{II}(salen^{\bullet+})$ complex, the transition from fully delocalized class III to localized class II occurs upon the exchange of the *t*-Bu substituent to the MeO substituent on the salen ligand, possibly due to the difference in the redox potential. The present findings point to a fascinating possibility that electron transfer could be drastically modulated by exchanging the metal ion that bridges the two redox centers or by adjusting the redox potential of the electron donor and acceptor relative to the metal ion mediator.

EXPERIMENTAL SECTION: INSTRUMENTATION

Absorption spectra in the range from 200 to 1100 nm were recorded on an Agilent 8453 spectrometer (Agilent Technologies) equipped with a USP-203 low-temperature chamber (UNISOKU). Absorption spectra in the range from 200 to 3200 nm were recorded on a UV-3150 UV–vis–NIR spectrophotometer (Shimadzu) equipped with a USP-203 low-temperature chamber (UNISOKU). Quartz cells (l = 0.05 cm), which are fitted for the low-temperature chamber, were custom-made by domestic glassware manufacturers (Eikosha and Agri). Electrochemical oxidation was conducted using a gold-mesh working electrode, a platinum-wire counter electrode, and a Ag/AgCl reference electrode, which are connected to an HA-151 potentiostat–galvanostat (Hokuto Denko). The gold mesh, silver rod, and platinum wire and sheet were obtained from Nilaco. Electron paramagnetic resonance (EPR) spectra were recorded for 30 μL of the 10 mM frozen CH_2Cl_2 solution containing 1.0 M Bu_4NOTf at 4 K in a quartz tube (o.d. = 5 mm) on an E500 continuous-wave X-band spectrometer (Bruker) with an ESR910 helium-flow cryostat (Oxford Instruments). EPR spectra of one-electron-oxidized Ni^{II}(salen) complexes were recorded for 20 μL of the 5 mM CH_2Cl_2 solution at room temperature. Cyclic voltammograms were measured with an ALS612A electrochemical analyzer (BAS). A saturated calomel reference electrode, a glassy carbon working electrode, and a platinum-wire counter electrode were utilized. Measurements were carried out for the 1 mM solution in dehydrated CH_2Cl_2 containing 0.1 M Bu_4NOTf at a scan rate of 50 mV s^{-1} at 233 K under an Ar atmosphere. The E values were referenced to the $E_{1/2}$ value of ferrocene, which was measured under identical conditions. Solid-state magnetic susceptibility measurements were made by using an MPMS-7 SQUID susceptometer (Quantum Design) operating in the 2–300 K temperature range. Well-ground polycrystalline samples were wrapped in a plastic sheet and were loaded into the sample folder (a drinking straw). The susceptibilities of the plastic sheet and the sample folder were measured in the same temperature range and field to provide an accurate correction for its contribution to the total magnetic susceptibility. Diamagnetic corrections were estimated from Pascal constants. NMR (500 and 400 MHz) spectra were measured in a borosilicate glass tube (o.d. = 5 mm) on LA-500 and LA-400 spectrometers (JEOL), respectively. ^{1}H NMR chemical shifts in CD_2Cl_2 and $CDCl_3$ were referenced to $CHDCl_2$ (5.32 ppm) and $CHCl_3$ (7.24 ppm), respectively. ^{13}C NMR chemical shifts in $CDCl_3$ were reported relative to $CHCl_3$ (77.0 ppm). ESI-MS spectra were obtained with an LCT time-of-flight mass spectrometer equipped with an electrospray ionization interface (Micromass). Elemental analyses were conducted on a CHN corder MT-6 (Yanaco). High-resolution mass spectra were measured with the JMS-777V mass spectrometer (JEOL). High-performance liquid chromatography was carried out on an LC-9201 instrument (Japan Analytical Industry) with JAIGEL-1H and JAIGEL-2H using $CHCl_3$ as the eluent.

ASSOCIATED CONTENT

Supporting Information. Synthetic details and Figures S1–S18. This material is available free of charge via the Internet at http://pubs.acs.org.

AUTHOR INFORMATION

Corresponding Author
hiro@ims.ac.jp

ACKNOWLEDGMENT

We thank Mr. Seiji Makita (Institute for Molecular Science) for elemental analysis and measurements of high-resolution mass spectrometry. This study was supported by a grant from Japan Society for the Promotion of Science (Grant-in-Aid for Science Research, Grant No. 22350030).

REFERENCES

(1) (a) Nelsen, S. F. *Chem.—Eur. J.* **2000**, *6*, 581–588. (b) Nishihara, H. *Bull. Chem. Soc. Jpn.* **2001**, *74*, 19–29. (c) Demadis, K. D.; Hartshorn, C. M.; Meyer, T. J. *Chem. Rev.* **2001**, *101*, 2655–2685. (d) Brunschwig, B. S.; Creutz, C.; Sutin, N. *Chem. Soc. Rev.* **2002**, *31*, 168–184. (e) Evangelio, E.; Ruiz-Molina, D. *Eur. J. Inorg. Chem.* **2005**, 2957–2971.

(f) D'Alessandro, D. M.; Keene, F. R. *Chem. Soc. Rev.* **2006**, *35*, 424–440. (g) D'Alessandro, D. M.; Keene, F. R. *Chem. Rev.* **2006**, *106*, 2270–2298. (h) Chisholm, M. H.; Patmore, N. J. *Acc. Chem. Res.* **2007**, *40*, 19–27. (i) Kaim, W.; Lahiri, G. K. *Angew. Chem., Int. Ed.* **2007**, *46*, 1778–1796. (j) Glover, S. D.; Goeltz, J. C.; Lear, B. J.; Kubiak, C. P. *Eur. J. Inorg. Chem.* **2009**, 585–594.

(2) (a) Creutz, C.; Taube, H. *J. Am. Chem. Soc.* **1969**, *91*, 3988–3989. (b) Creutz, C.; Taube, H. *J. Am. Chem. Soc.* **1973**, *95*, 1086–1094.

(3) Robin, M. B.; Day, P. *Adv. Inorg. Chem. Radiochem.* **1967**, *10*, 247–422.

(4) (a) Hush, N. S. *Prog. Inorg. Chem.* **1967**, *8*, 391–444. (b) Hush, N. S. *Electrochim. Acta* **1968**, *13*, 1005–1023.

(5) (a) Rosokha, S. V.; Neretin, I. S.; Sun, D.; Kochi, J. K. *J. Am. Chem. Soc.* **2006**, *128*, 9394–9407. (b) Santi, S.; Orian, L.; Donoli, A.; Bisello, A.; Scapinello, M.; Benetollo, F.; Ganis, P.; Ceccon, A. *Angew. Chem., Int. Ed.* **2008**, *47*, 5331–5334. (c) Das, A. K.; Sarkar, B.; Fiedler, J.; Zális, S.; Hartenbach, I.; Strobel, S.; Lahiri, G. K.; Kaim, W. *J. Am. Chem. Soc.* **2009**, *131*, 8895–8902. (c) Olivier, C.; Costuas, K.; Choua, S.; Maurel, V.; Turek, P.; Saillard, J.-Y.; Touchard, D.; Rigaut, S. *J. Am. Chem. Soc.* **2010**, *132*, 5638–5651.

(6) (a) Pierpont, C. G.; Lange, C. W. *Prog. Inorg. Chem.* **1994**, *41*, 331–442. (b) Adams, D. M.; Hendrickson, D. N. *J. Am. Chem. Soc.* **1996**, *118*, 11515–11528. (c) Chang, H.-C.; Miyasaka, H.; Kitagawa, S. *Inorg. Chem.* **2001**, *40*, 146–156.

(7) (a) Herebian, D.; Bothe, E.; Neese, F.; Weyhermüller, T.; Wieghardt, K. *J. Am. Chem. Soc.* **2003**, *125*, 9116–9128. (b) Chlopek, K.; Bothe, E.; Neese, F.; Weyhermüller, T.; Wieghardt, K. *Inorg. Chem.* **2006**, *45*, 6298–6307.

(8) (a) Ray, K.; Weyhermüller, T.; Neese, F.; Wieghardt, K. *Inorg. Chem.* **2005**, *44*, 5345–5360. (b) Ray, K.; Bill, E.; Weyhermüller, T.; Wieghardt, K. *J. Am. Chem. Soc.* **2005**, *127*, 5641–5654.

(9) (a) Bill, E.; Bothe, E.; Chaundhuri, P.; Chlopek, K.; Herebian, D.; Kokatam, S.; Ray, K.; Weyhermüller, T.; Neese, F.; Wieghardt, K. *Chem.—Eur. J.* **2005**, *11*, 204–224. (b) Kokatam, S.; Weyhermüller, T.; Bothe, E.; Chaundhuri, P.; Wieghardt, K. *Inorg. Chem.* **2005**, *44*, 3709–3717.

(10) Lu, C. C.; Bill, E.; Weyhermüller, T.; Bothe, E.; Wieghardt, K. *J. Am. Chem. Soc.* **2008**, *130*, 3181–3197.

(11) (a) Pratt, R. C.; Stack, T. D. P. *J. Am. Chem. Soc.* **2003**, *125*, 8716–8717. (b) Shimazaki, Y.; Tani, F.; Fukui, K.; Naruta, Y.; Yamauchi, O. *J. Am. Chem. Soc.* **2003**, *125*, 10512–10513. (c) Rotthaus, O.; Jarjayes, O.; Thomas, F.; Philouze, C.; Perez Del Valle, C.; Saint-Aman, E.; Pierre, J.-L. *Chem.—Eur. J.* **2006**, *12*, 2293–2302. (d) Rotthaus, O.; Thomas, F.; Jarjayes, O.; Philouze, C.; Saint-Aman, E.; Pierre, J.-L. *Chem.—Eur. J.* **2006**, *12*, 6953–6962. (e) Shimazaki, Y.; Yajima, T.; Tani, F.; Karasawa, S.; Fukui, K.; Naruta, Y.; Yamauchi, O. *J. Am. Chem. Soc.* **2007**, *129*, 2559–2568. (f) Benisvy, L.; Kannappan, R.; Song, Y.-F.; Milikisyants, S.; Huber, M.; Mutikainen, I.; Turpeinen, U.; Gamez, P.; Bernasconi, L.; Baerends, E. J.; Hartl, F.; Reedijk, J. *Eur. J. Inorg. Chem.* **2007**, 637–642. (g) Rotthaus, O.; Jarjayes, O.; Perez Del Valle, C.; Philouze, C.; Thomas, F. *Chem. Commun.* **2007**, 4462–4464. (h) Storr, T.; Wasinger, E. C.; Pratt, R. C.; Stack, T. D. P. *Angew. Chem., Int. Ed.* **2007**, *46*, 5198–5201. (i) Storr, T.; Verma, P.; Pratt, R. C.; Wasinger, E. C.; Shimazaki, Y.; Stack, T. D. P. *J. Am. Chem. Soc.* **2008**, *130*, 15448–15459. (j) Shimazaki, Y.; Stack, T. D. P.; Storr, T. *Inorg. Chem.* **2009**, *48*, 8383–8392. (k) Orio, M.; Jarjayes, O.; Kanso, H.; Philouze, C.; Neese, F.; Thomas, F. *Angew. Chem., Int. Ed.* **2010**, *49*, 4989–4992. (l) Kochem, A.; Orio, M.; Jarjayes, O.; Neese, F.; Thomas, F. *Chem. Commun.* **2010**, 6765–6767. (m) Storr, T.; Verma, P.; Shimazaki, Y.; Wasinger, E. C.; Stack, T. D. P. *Chem.—Eur. J.* **2010**, *16*, 8980–8983.

(12) Ray, K.; Petrenko, T.; Wieghardt, K.; Neese, F. *Dalton Trans.* **2007**, 1552–1566.

(13) McGarrigle, E. M.; Gilheany, D. G. *Chem. Rev.* **2005**, *105*, 1563–1602.

(14) (a) Kurahashi, T.; Kobayashi, Y.; Nagatomo, S.; Tosha, T.; Kitagawa, T.; Fujii, H. *Inorg. Chem.* **2005**, *44*, 8156–8166. (b) Kurahashi, T.; Kikuchi, A.; Tosha, T.; Shiro, Y.; Kitagawa, T.; Fujii, H. *Inorg. Chem.* **2008**, *47*, 1674–1686. (c) Kurahashi, T.; Fujii, H. *Inorg. Chem.* **2008**, *47*, 7556–7567. (d) Kurahashi, T.; Hada, M.; Fujii, H. *J. Am. Chem. Soc.* **2009**, *131*, 12394–12405. (e) Kurahashi, T.; Kikuchi, A.; Shiro, Y.; Hada, M.; Fujii, H. *Inorg. Chem.* **2010**, *49*, 6664–6672.

(15) (a) Müller, J.; Kikuchi, A.; Bill, E.; Weyhermüller, T.; Hildebrandt, P.; Ould-Moussa, L.; Wieghardt, K. *Inorg. Chim. Acta* **2000**, *297*, 265–277. (b) Mukherjee, S.; Weyhermüller, T.; Bothe, E.; Wieghardt, K.; Chaudhuri, P. *Dalton Trans.* **2004**, 3842–3853.

(16) (a) Matsushita, T.; Hirata, Y.; Shono, T. *Bull. Chem. Soc. Jpn.* **1982**, *55*, 108–112. (b) Okawa, H.; Nakamura, M.; Kida, S. *Bull. Chem. Soc. Jpn.* **1982**, *55*, 466–470. (c) Chin, D.-H.; Saywer, D. T.; Schaefer, W. P.; Simmons, C. J. *Inorg. Chem.* **1983**, *22*, 752–758. (d) Hartman, J. R.; Foxman, B. M.; Cooper, S. R. *Inorg. Chem.* **1984**, *23*, 1381–1387. (e) Lynch, M. W.; Hendrickson, D. N.; Fitzgerald, B. J.; Pierpont, C. G. *J. Am. Chem. Soc.* **1984**, *106*, 2041–2049. (f) Tirant, M.; Smith, T. D. *Inorg. Chim. Acta* **1986**, *121*, 5–11. (g) Kessissoglou, D. P.; Li, X.; Butler, W. M.; Pecoraro, V. L. *Inorg. Chem.* **1987**, *26*, 2487–2492. (h) Chandra, S. K.; Basu, P.; Ray, D.; Pal, S.; Chakravorty, A. *Inorg. Chem.* **1990**, *29*, 2423–2428. (i) Mikuriya, M.; Jie, D.; Kakuta, Y.; Tokii, T. *Bull. Chem. Soc. Jpn.* **1993**, *66*, 1132–1139. (j) Adam, B.; Bill, E.; Bothe, E.; Goerdt, B.; Haselhorst, G.; Hildenbrand, K.; Sokolowski, A.; Steenken, S.; Weyhermüller, T.; Wieghardt, K. *Chem.—Eur. J.* **1997**, *3*, 308–319.

(17) Chaudhuri, P.; Wieghardt, K. *Prog. Inorg. Chem.* **2001**, *50*, 151–216.

(18) Wieghardt et al. recently reported a similar observation in their bis(α-iminopyridine)metal system, in which zinc(II), chromium(II), and manganese(II) ions give rise to a class I ligand radical, while iron(II) and cobalt(II) ions give rise to a fully delocalized class III ligand radical. See ref 10.